A New Parameter to Control Heat Transport in Nanofluids: Surface Charge State of the Particle in Suspension

Donggeun Lee,*,† Jae-Won Kim,† and Bog G. Kim‡

School of Mechanical Engineering and Department of Physics, Pusan National University, Busan 609-735, Korea

Received: December 10, 2005; In Final Form: January 17, 2006

Although various conjectures have been proposed to explain the abnormal increase in thermal conductivity of nanofluids, the detailed mechanism has not been fully understood and explained. The main reason is due to the lack of knowledge of the most fundamental factor governing the mechanisms such as Brownian motion, liquid layering, phonon transport, surface chemical effects, and agglomeration. Applying a surface complexation model for the measurement data of hydrodynamic size, ζ potential, and thermal conductivity, we have shown that surface charge states are mainly responsible for the increase in the present condition and may be the factor incorporating all the mechanisms as well.

1. Introduction

Together with the greatly increasing thermal load in microelectronics and higher-powered automobiles, the needs for high-performance cooling fluids are increasing every year. As conventional approaches using extended surfaces required additional pumping power and were thought to have reached their limits, various attempts to increase thermal conductivity of the fluid itself have been made. Since 1995 when U. S. Choi showed the possibility of using a new type of fluid containing nanoparticles,[1] large enhancements of up to more than 100% in effective thermal conductivity (K_{eff}) of such fluids have been reported. The promising prospect for the fluid, *nanofluids*, triggered many researchers to find the best combination of particles and solvents[2−10] and to elucidate the governing mechanisms[11−16] as well.

Keblinski et al.[13] suggested three possible mechanisms responsible for the abnormal increase: Brownian motion of particles, liquid layering, and ballistic phonon transport. They seemed likely to give a reasonable insight into what the most important factor affecting the K_{eff} is. Although they showed that the effect of Brownian motion was negligible by scaling analysis, a few authors are still arguing the influence. For examples, Jang and Choi[14] and Kumar et al.[15] derived their own formulas to consider the nanoconvection caused by Brownian motion. They both predicted the K_{eff} nicely using different equations (also see the comments on the work of Kumar et al.: [15] *Phys. Rev. Lett.* **2005**, *95*, 019401 and 209401). Also, they disregarded that metal oxide particles used for the validation of the Brownian models were highly aggregated (see ref 16 in Jang and Choi[14] and ref 14 in Kumar et al.[15]). As such, aggregate particles move much more slowly than the isolated ones do; their mobility equivalent size (often called hydrodynamic size) should be used rather than the primary particle size.

On the other hand, some people[13,16,17] claimed the liquid layering at the particle−liquid interface to be most important and supported its validity by predicting the K_{eff} with their models. However, it should be noted that their estimations were based on arbitrarily assumed values for thermal conductivity and thickness of the interfacial layer. Moreover, there is no available theory and experimental data for discussing the ballistic phonon transport quantitatively.

Two groups[10,7] added one more important factor, i.e., surface chemical effect, which is not understood by all pre-existing models. Xie et al.[10] showed that just simple acid treatment of carbon nanotubes[10] enhanced the suspension stability of carbon nanotube in water. It was attributed to hydrophobic-to-hydrophilic conversion of the surface nature due to the generation of a hydroxyl group. Patel et al.[7] reported that 4 nm Au nanoparticles with a coating of a covalent chain in toluene were about 50 times less effective for heat transport than uncoated 10−20 nm Au particles in water. This is exactly contrary to the conventional size effect.[8,14,15]

Because of the aforementioned complexity and contradiction in nanofluids, the research community has not reached a solid consensus on the mechanisms. Here, we take notice of the suspension stability as a common factor in the current technological limitations. As the colloidal system becomes less stable, particles are aggregated, leading to changes in the hydrodynamic size as well as morphology and sometimes in volume fraction by settling out. Note that the surface chemical treatment changes the suspension stability through surface charge states and resultant surface potential.[18,19]

Therefore, we attempt in this work to clarify the role of surface charge states as a most fundamental factor. We change pH of the solution systematically to control surface charge density and surface potential that can be reflected by ζ potential. Employing the surface complexation model,[18,19] we obtain all relevant surface charge states from the measured values of the ζ potential and hydrodynamic size of CuO−water nanofluids at various pH conditions. The corresponding suspension stability is quantified from the data through the Derjaguin−Landau−Verwey−Overbeek (DLVO) linearized mean field theory.[18] We find that higher surface charges facilitate heat transport more effectively. On the basis of the result, we propose another key

* To whom correspondence should be addressed. Electronic mail: donglee@pusan.ac.kr. Tel.: +82-51-510-2365. Fax: +82-51-512-5236.
† School of Mechanical Engineering.
‡ Department of Physics.

10.1021/jp057225m CCC: $33.50
Published on Web 02/11/2006

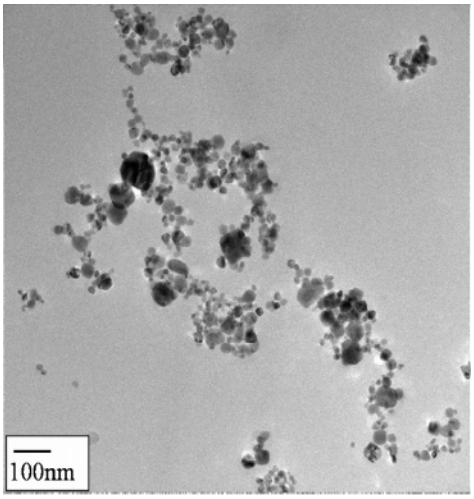

Figure 1. TEM micrograph of CuO nanoparticles prepared by rapid drying of a diluted sample.

role of the surface charge states as a supply of path and efficiency for phonon transport.

2. Experimental Section

A. Preparation of Nanofluid. Commercial CuO particles from Aldrich are chosen as a source material for a nanofluid. Three things for the selection were considered for the selection. First, deionized (DI) water is nontoxic and one of the most common fluids for general-purpose cooling. Second, particles should then be well-suspended in the base fluid (water) at neutral condition (pH = 7) (will be shown later). Finally, we considered how much available data we could find for evaluation of the measurement accuracy. Data on the thermal conductivity of the CuO nanofluid have been frequently reported and referenced by many pre-existing articles.[2,3,5,11,14−17]

CuO particles as received from Aldrich are highly aggregated, and their primary size is estimated at a mean diameter of ~25 nm. As a first step, the pH of deionized water as a base fluid is adjusted by adding suitable amounts of HCl or NaOH. Then, the particles are immersed into DI water maintained at various pHs. The pH of the solution is again measured with a pH meter. The pH of the solution is slightly shifted to lower value from that of the base fluid, which means the surfaces of the CuO particles are slightly acid-terminated. The volume fraction of particles is kept constant at 0.3 vol % during the whole experiments unless otherwise noticed.

To get the better suspension, colloidal particles are mechanically torn into a smaller size with a 700 W ultrasonicator, but the ultrasonic treatment seems not to be enough. Despite many tests on different duration and power of the ultrasonication, the particles sustain their fractal shapes as seen in Figure 1. The sample for transmission electron microscopy (TEM) is prepared by diluting the nanofluids with enough base fluid, sampling the solution on top of the TEM grid, and subsequently rapidly drying the grid. The traditional photon correlation method[18] (Otsuka Co., Japan) is used to double-check that the particles in water behave like big clusters consisting of small primary particles. As the measured diffusion coefficient of the particles yields the hydrodynamic size through the Stokes−Einstein equation, the size should best describe the Brownian motion or nanoconvective motion. The measured size ranges from 160 to 280 nm at different pH conditions in Figure 2. The size seems to already be too large to cause any Brownian effect (will be discussed later), which again confirms that the particles are aggregated.

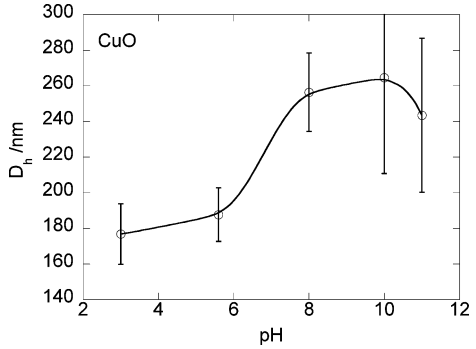

Figure 2. Hydrodynamic sizes of nanoparticles in suspension at different pHs of the solution.

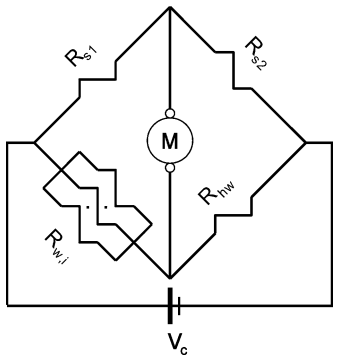

Figure 3. Schematic of transient hot wire method for the measurement of effective thermal conductivity of nanofluids.

B. Measurement of the Effective Thermal Conductivity of Nanofluid. Thermal conductivity of the nanofluid is measured at 25 °C by a conventional transient hot wire device[2−4,8] equipped with a homemade wheatstone bridge. As seen in Figure 3, the device consists of a digital multimeter, a stable dc power supply, and electrical resistances including a Teflon-coated Pt wire of 70 μm diameter. They are symbolized in the figure by M, V_c, and R, respectively. The subscript "s" represents standard electrical resistance, "hw" indicates the Pt hot wire, and "wi" represents a unit of parallel connections of several standard electrical resistances. Note that the parallel connections of different standard resistances of 2, 4, 8, 16, 32, 64, ... ohms make it possible to replace a variable resistance with sufficient resolution and stability.

The working principle of such a hot wire method is well-established and simple as follows. As soon as the voltage V_c is supplied to the wire, the temperature of the wire begins to increase, resulting in an increase of the R_{hw}. Concurrent transient changes of the bridge output are recorded by the multimeter. Nagasaka and Nagashima[20] derived an approximated solution for the one-dimensional transient heat conduction from a thin wire with a coating

$$T(t) - T_0 \approx \frac{q}{4\pi k}(\ln t + C) \qquad (1)$$

where $T(t) - T_0$ is the temperature rise of the wire from the beginning of the heating, q is the applied electrical power, C is a constant, and k corresponds to the K_{eff} of the nanofluid. The relationship given by eq 1 implies a straight line for a plot of $T - T_0$ against $\ln(t)$. The K_{eff} is obtained from the slope of the line. As far as the enhancement of K_{eff} with respect to the base fluid (K_{eff}/K_f) concerns, one may have to know the variations of K_f at different pHs. We made the same solution with no particles like the nanofluids at different pHs and measured the

K_f. Interestingly, we find that the K_f of the solution is nearly constant even when dissolving small amounts of salt or acid.

To minimize any inconsistency in experiments arising from suspension instability (at low ζ), all measurements are performed exactly 30 min after making a fresh nanofluid. The time is likely too short for settling to begin, but long enough to calm down the initial disturbance of fluid, because sediments at the bottom were hardly seen even for low ζ at this time. During the experiments, the ionic strength of nanofluids is kept nearly constant using a symmetric 1:1 electrolyte $(NaCl)_{aq}$ of 5×10^{-4} mol dm^{-3} (far less than the critical coagulation concentration of 5×10^{-2} mol dm^{-3} in this case), so it is unlikely for particles to settle down via agglomeration. We measure the hydrodynamic diameter (D_h) of particles in liquid by measuring the diffusion coefficient with photon correlation spectroscopy.[18] The ζ potential of the nanofluid is also measured from electrokinetic data using a commercial instrument (Otsuka Co., Japan).

3. Surface Complexation (SC) Model

When materials such as oxides, sulfides, and insoluble salts are immersed in aqueous solution, they acquire a surface charge due to the protonation or deprotonation process of a surface group such as a hydroxyl ligand (−OH) of the metal oxide as follows:[18,19]

$$\mathrm{MOH} + \mathrm{H}^+ \xrightarrow[K_p]{} \mathrm{MOH_2}^+ \quad K_p = \exp\left(\frac{F\psi_0}{RT}\right)\frac{\Gamma(\mathrm{MOH_2}^+)}{a(\mathrm{H}^+)\Gamma(\mathrm{MOH})}$$

$$\mathrm{MOH} \xrightarrow[K_d]{} \mathrm{MO}^- + \mathrm{H}^+ \quad K_d = \exp\left(-\frac{F\psi_0}{RT}\right)\frac{\Gamma(\mathrm{MO}^-)a(\mathrm{H}^+)}{\Gamma(\mathrm{MOH})} \tag{2}$$

where M is a metal cation, i.e., Cu(II) in this case, K_p and K_d are intrinsic equilibrium constants for protonation and deprotonation, respectively, a is activity in the bulk of the solution, ψ_0 is the surface potential affecting the number of charged surface groups MOH_2^+ and MO^-, and Γ is a site density of the surface groups. Counterions, with opposite polarity in liquid, are attracted to bond strongly to the surface charged group, resulting in a decrease of the potential in the stern layer ($0 < x < d$) in Figure 4. The adsorption of such indifferent ions is expressed by

$$\mathrm{MOH_2}^+ + \mathrm{A}^- \xrightarrow[K_a]{} \mathrm{MOH_2}^+\cdot\mathrm{A}^- \quad K_a = \exp\left(-\frac{F\psi_\beta}{RT}\right)\frac{\Gamma(\mathrm{MOH_2}^+\cdot\mathrm{A}^-)}{a(\mathrm{A}^-)\Gamma^*(\mathrm{MOH_2}^+)}$$

$$\mathrm{MO}^- + \mathrm{C}^+ \xrightarrow[K_d]{} \mathrm{MO}^-\cdot\mathrm{C}^+ \quad K_d = \exp\left(\frac{F\psi_\beta}{RT}\right)\frac{\Gamma(\mathrm{MO}^-\cdot\mathrm{C}^+)}{a(\mathrm{C}^+)\Gamma^*(\mathrm{MO}^-)} \tag{3}$$

where A^- and C^+ correspond to Na^+ and Cl^- in this study, respectively. Note that some of the parent sites ($\Gamma(MOH_2^+)$ and $\Gamma(MO^-)$) in eq 2 are subsequently divided via the adsorption into four sites, i.e., $\Gamma^*(MOH_2^+)$, $\Gamma^*(MO^-)$, $\Gamma(MOH_2^+\cdot A^-)$, and $\Gamma(MO^-\cdot C^+)$ at the second equilibrium. The total sum of the four site densities and $\Gamma(MOH)$ is equal to total surface site density Γ_{tot} implying how many atoms per unit area exist at the surface. The Γ_{tot} is estimated to be ca. 5.9×10^{-6} mol dm^{-3} (3.5 sites nm^{-2}) from the size of spherical primary particles and maintains constant at different pHs. With eqs 2 and 3, the uncharged site density ($\Gamma(MOH)$) can be obtained with given values of K_p, K_d, K_a, K_c, ψ_0, and ψ_β by

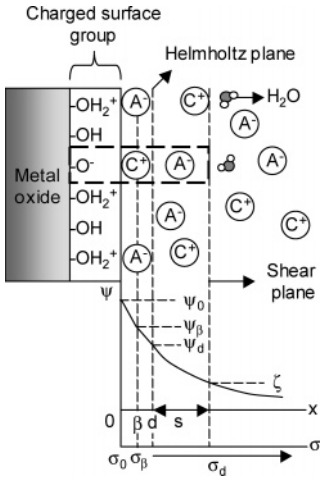

Figure 4. Structure of electrical double layer (EDL) formed at the metal oxide−water interface. Dehydrated counterion A^- or C^+ bonds strongly to the charged group at surface, forming an immobile part of the EDL (stern layer). In contrast, in the outer region, such ions are bound weakly, resulting in gradual decrease in the potential. The outer layer is called a diffuse layer. The Helmholtz plane at $x = d$ is a border between a stern layer ($0 < x < d$) and a diffuse layer ($x > d$). At the shear plane (at $x = d + s$), the ζ potential is measured. C and A are acronyms for cation and anion as counterparts of potential-determining ions (OH^- and H^+), respectively.

$$\frac{\Gamma_{tot}}{\Gamma(\mathrm{MOH})} = 1 + \frac{a(\mathrm{H}^+)K_p\exp\left(-\frac{F\psi_0}{RT}\right)}{1 + K_a a(\mathrm{A}^-)\exp\left(\frac{F\psi_\beta}{RT}\right)} + \frac{K_d/a(\mathrm{H}^+)\exp\left(\frac{F\psi_0}{RT}\right)}{1 + K_c a(\mathrm{C}^+)\exp\left(-\frac{F\psi_\beta}{RT}\right)} + \frac{a(\mathrm{H}^+)K_p\exp\left(-\frac{F\psi_0}{RT}\right)}{1 + K_a a(\mathrm{A}^-)\exp\left(\frac{F\psi_\beta}{RT}\right)}a(\mathrm{A}^-)K_a\exp\left(\frac{F\psi_\beta}{RT}\right) + \frac{K_d/a(\mathrm{H}^+)\exp\left(\frac{F\psi_0}{RT}\right)}{1 + K_c a(\mathrm{C}^+)\exp\left(-\frac{F\psi_\beta}{RT}\right)}a(\mathrm{C}^+)K_c\exp\left(-\frac{F\psi_\beta}{RT}\right) \tag{4}$$

The surface charge densities in 0- and β-planes (σ_0 and σ_β) are

$$\sigma_0 = F[\Gamma(\mathrm{MOH_2}^+) + \Gamma(\mathrm{MOH_2}^+\cdot\mathrm{A}^-) - \Gamma(\mathrm{MO}^-) - \Gamma(\mathrm{MO}^-\cdot\mathrm{C}^+)]$$

$$\sigma_\beta = F[\Gamma(\mathrm{MO}^-\cdot\mathrm{C}^+) - \Gamma(\mathrm{MOH_2}^+\cdot\mathrm{A}^-)] \tag{5}$$

In the triple-layer model,[19] the net surface charge density σ_s, corresponding to the charge fixed to the surface, is balanced with that in the diffuse layer (σ_d) given by solving the Poisson equation

$$\sigma_s = \sigma_0 + \sigma_\beta = F[\Gamma(\mathrm{MOH_2}^+) - \Gamma(\mathrm{MO}^-)] = -\sigma_d = -\frac{4FI}{\kappa}\sinh\left(\frac{F\psi_\beta}{2RT}\right) \tag{6}$$

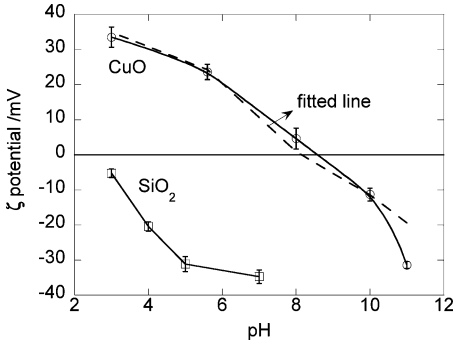

Figure 5. Change of ζ potentials of CuO and SiO_2 with pH; the error bars denote standard deviations of data from more than ten measurements.

TABLE 1: Parameters Used for the Estimation of the ζ Potential

$K_p = 6 \times 10^4$ mol^{-1} dm^3
$K_d = 2 \times 10^{-12}$ mol dm^{-3}
$K_a = 10$ mol^{-1} dm^3
$K_c = 1$ mol^{-1} dm^3
$K_w = 1 \times 10^{-14}$ mol^2 dm^{-6}
$F = 96\,485$ C mol^{-1}
$R = 8.31$ J mol^{-1} K^{-1}
$T = 298$ K
$\epsilon_0 = 8.854 \times 10^{-12}$ C V^{-1} m^{-1}
$\epsilon_r = 80$ for water

where I is the ionic strength, F is the Faraday constant, ψ_β is essentially very close to ψ_d, and the reciprocal Debye−Huckel parameter κ^{-1} ($=\sqrt{\epsilon_0\epsilon_r RT/2000F^2 I}$) often scales as the thickness of the electrical double layer. The ψ_0 can be approximated to the Nernst potential ψ_N ($=\log[a(H^+)/a_{pzc}(H^+)]RT/F$) with 90% accuracy.[19]

The fitting process is as follows:

(1) Obtain ψ_0 ($\approx\psi_N$) and ψ_β ($\approx\psi_d$) from the measured ζ by Gouy−Chapmann (GC) theory

$$\tanh(F\zeta/4RT) = \tanh(F\psi_d/4RT)\exp(-\kappa s)$$

(2) Obtain the uncharged site density Γ(MOH) using eq 4 with presumed equilibrium constants of K_p, K_d, K_a, and K_c.

(3) Obtain all charged site densities from eqs 2 and 3.

(4) Estimate the surface charge densities σ_0 and σ_β from eqs 5 and 6.

(5) Estimate the ψ_β ($\approx\psi_d$) and ζ by applying eq 6 and GC theory to the σ_s and ψ_d, respectively.

(6) Try different values for the four equilibrium constants and repeat steps 2−5 until the estimated ζ gets closest to the measured ζ.

4. Results and Discussion

A. Influence of pH on the ζ Potential and Surface Charge States. Figure 5 shows the changes of ζ potential for SiO_2− and CuO−water nanofluids as a fuction of pH. Isoelectric points (IEP), the pH values at which ζ is zero, agree well with literature values for two materials (2−4 for SiO_2; 8.5−9.5 for CuO).[21] Since K_p and K_d for CuO have not been reported, we iterate to the prescribed fitting process with various values. The prediction of the ζ potential at $K_p = 6 \times 10^4$ mol^{-1} dm^3 and $K_d = 2 \times 10^{-12}$ mol dm^{-3} is best. The dotted line in the figure represents the estimation of the ζ potential. All parameters for the best fit are listed in Table 1.

To check whether these parameters are physically reasonable, a value of 0.5 log(K_p/K_d) from the taken values is compared to the point of zero charge (PZC) cited in the literature.[21] These two values should essentially coincide with each other.[18] The value of 0.5 log(K_p/K_d) (ca. 8.3) lies within a reasonable range of the point of zero charge for CuO. As the pH goes away from the PZC, the surface charge or site density (σ or Γ) increases because of more frequent attacks to the surface hydroxyl groups by potential-determining ions (PDI: H^+ and OH^-), leading to an increase in ψ_0, ψ_d, and ζ. In this way, we can estimate all surface charge states such as the surface charge densities and charged surface site densities (Γ) and present the Γs in Figure 6. As expected, the total charged site density ($\Gamma_{tot} - \Gamma$(MOH)) is minimum at the PZC. The choice of K_a and K_c does not generate any considerable change in the total charged site density (the meaning will be discussed later). The fraction of total charged sites ($1 - \Gamma(MOH)/\Gamma_{tot}$) varies from 7×10^{-4} to 2.4×10^{-1} as pH decreases from PZC; the majority of amphoteric sites are uncharged especially at PZC.[18]

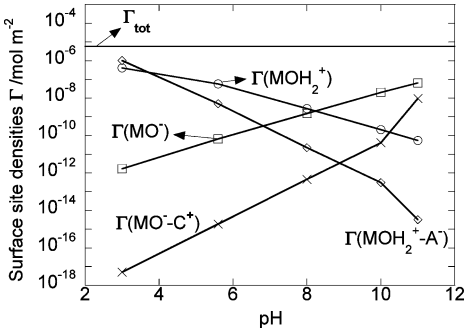

Figure 6. The site densities of charged surface species at different pHs.

B. Influence of pH on Suspension Stability of Nanofluid. Particles in liquid suspension attract or repel each other, depending on total interaction energy E_{tot} that is the sum of the van der Waals attraction E_A and the electrostatic repulsion E_{el} between them. The E_{el} between two charged particles with the surface potentials ψ_{d1} and ψ_{d2} is approximated by the DLVO theory[18,19]

$$E_{el} = \frac{\epsilon_0\epsilon_r r_1 r_2}{r_1 + r_2}\left\{2\psi_{d1}\psi_{d2}\ln\left[\frac{1+\exp(-\kappa x)}{1-\exp(-\kappa x)}\right] + (\psi_{d1}{}^2 + \psi_{d1}{}^2)\ln[1-\exp(-2\kappa x)]\right\} \quad (7)$$

where r is the radii of particles, x is a interparticle surface-to-surface distance, and the others have conventional meanings. It is obvious that the higher the potentials (ψ_d or ζ) are, the bigger the potential barrier for agglomeration gets. At the 0.3 vol % dose of particles, the interparticle distance is about 100 nm for mobility-equivalent spherical particles. At this condition, the second term in the bracket of eq 7 is negligible compared to the first. Thus, the repulsion energy of the same-sized particles goes up approximately in proportion to ζ^2.

The attraction energy between the same particles is given by the Hamaker equation: $E_A = -A_{132}r/(12x)$. The Hamaker constant A_{132} of metal oxide is typically on the order of 10^{-20} J.[18,22] With eq 7, the Hamaker equation, and the estimated ψ_d, E_{tot} is calculated as a function of x at different pHs as shown in Figure 7. In the present condition, the repulsion barrier gets bigger than the attraction as pH goes from PZC, which makes the colloids more stable. At pH 8 or 10 when ζ is small, however, the repulsion barrier disappears, and particles are subjected to only attraction. Strong particle agglomeration is expected in that case.

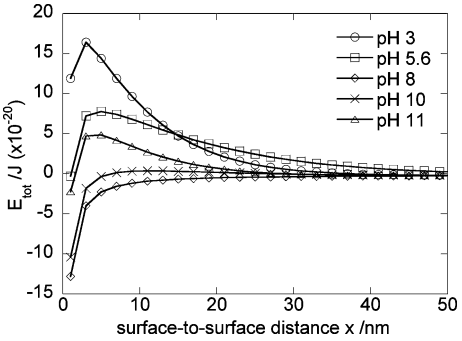

Figure 7. The interaction potentials at various pHs as a function of interparticle distance.

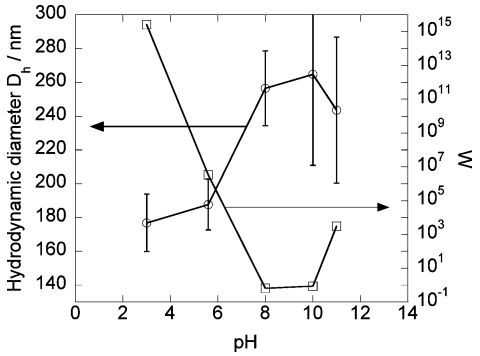

Figure 8. Relationship between the hydrodynamic size and stability coefficient at various pHs.

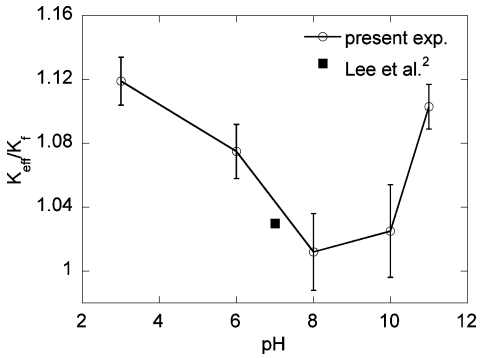

Figure 9. Effect of pH on the effective thermal conductivity of the CuO−water nanofluid.

Here, we need to quantify the suspension stability in terms of collision efficiency α that is responsible for colloidal particle growth. The α, a reciprocal value of stability coefficient *W*, is related to the rate constant of aggregation, $k = \alpha k_{diff} = k_{diff}/W$. The k_{diff} represents the rate constant of the coagulation between uncharged particles. N. Fucks derived a general relation of stability coefficient *W* to total interaction energy E_{tot}[18,19]

$$W = 2r\int_0^{\infty} \exp\left(\frac{E_{tot}}{k_b T}\right)\frac{dx}{(2r+x)^2} \qquad (8)$$

Figure 8 shows clearly that the *W* obtained by numerical integration of eq 8 is inversely proportional to the hydrodynamic diameter D_h at all pHs. This is the first report that the stability coefficient *W* can be used as a measure of suspension stability of nanofluids. The choice of the Hamaker constant does not yield big change of the relationship in the figure.

C. Influence of pH on Effective Thermal Conductivity of Nanofluid. Figure 9 shows that the effective thermal conductivity (K_{eff}) increases by a factor of 3 as pH decreases from 8 to 3. As addressed in the Introduction, such abnormal enhancements are not explained by any pre-existing model. Note that the thermal conductivity of base fluid is nearly constant at different doses of electrolyte salt and acid or base. The enhancement seems to be related only to particles. Since the previous results for the CuO−water nanofluid are limited only for the neutral (pH = 7) condition, we displayed the result of Lee et al.[2] in the figure for comparison. At the same volume loading (0.3%), their result agrees with ours within experimental error. To support the pH effect shown in Figure 9, we decrease the volume loading of particles up to 0.03%. Interestingly, we find that the surface charging effect is indeed true over the whole range of volume fraction and present in Figure 10.

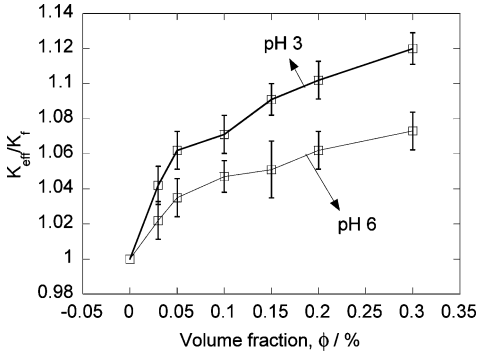

Figure 10. Variations of the effective thermal conductivity with increasing volume fraction at two different pHs.

Finally, we attempt to link the concept of surface charge states to the change in K_{eff} of nanofluids. The point to mention is that the charges seemingly transport heat more efficiently. We propose at this point a possible inference that the charged surface sites provide much more effective passages through which heats or phonons are going. As depicted in Figure 4, ionized surface groups at all charged sites (Γ_{ion}), regardless of their polarity, attract counterions (often hydrated). The latter again attract other indifferent ions in the outer region. This process may be repeated over and over, but the binding strength is likely decreasing. The alternating alignment of such ions may form cylindrical ordered structures consisting of molecule−ion liquid complexes, as depicted by a bold−dotted box in Figure 4. Polar liquid molecules are also likely to be tugged to the cylindrical columns.

In this way, as pH decreases from PZC, there are more surface sites (site density, Γ_{ion}) to launch the column and more available ions (ion density, $\sigma_d\kappa$) to strengthen the structure. Xue et al.[23] showed from molecular dynamic simulation that phonons felt much less resistance during travel from particle to liquid at stronger interfacial bonding. Therefore, it looks reasonable to infer that lower pH or higher surface charging condition facilitates phonon transport through increases of effective sites and transport efficiency. There is another aspect of the liquid column for heat transport. The ordered liquid structure is likely to mimic the original surface arrangement of solid atoms. As the number and strength of the columns increases with decreasing pHs, the columns may act as a part of the solid, leading to the effective increase of the volume fraction. If this is the case, the effective thermal conductivity K_{eff} may be expressed by a simple function of $\Gamma_{ion}\sigma_d\kappa$. Surprisingly, Figure 11 shows obviously the functional dependence that is close to a power law relationship. A different choice of unknown K_a and K_c does not change the relationship at all, because the Γ_{ion} is the sum of adsorbed and bare surface ionized groups. The previous concept of the interfacial layer may be related to the present figure. The thickness of the layer may scale as the thickness of the electrical double layer, i.e., κ^{-1}, while the thermal conduc-

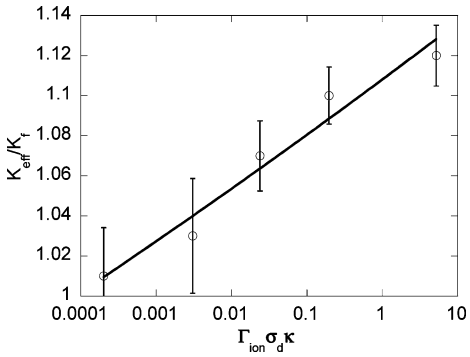

Figure 11. Strong correlation between the enhancement of the K_{eff} and the product of total charged site density and ion density.

tivity of the layer may be expressed by a power of the $\Gamma_{ion}\sigma_d\kappa$. This result may provide a new theoretical basis for determination of the nature of the interfacial layer for further development of an adequate model.

Changes in the sizes of colloidal particles as seen in Figure 8 can also change the K_{eff}, according to the nanoconvection model,[14,15] but the maximum increase estimated by applying the model of Kumar et al.[15] is on the order of 10^{-2}%, within the experimental uncertainty. This means that the size is already too large to cause any change in nanoconvection, but the primary particle size is still small enough to make the surface phenomena significant. Therefore, we conclude that the 12% increase of the K_{eff} is mainly due to the increase of the surface charge states.

Conclusions

We have shown that the pH of the colloidal liquid strongly affects the performance of the thermal fluid. As the pH of the solution goes far from the isoelectric point of particles, the colloidal particles get more stable and eventually alter the thermal conductivity of the fluid. We demonstrated that surface charge state is a basic parameter that is primarily responsible for the enhancement of thermal conductivity of the nanofluids. We proposed a new interpretation of the charged sites and ion densities in the diffuse layer as the number and efficiency of channels for phonon transport, respectively. The two concepts may offer a clue to draw solid conclusions on the mechanism issues. More, this study provides guidance for the manufacturing process of nanofluids: Higher surface charges and potentials are desirable. Second, we found that the surface charge states directly affected the suspension stability and presented the strong correlation between hydrodynamic size of particles and stability coefficient. However, the size effect on the heat transport was not significant.

Acknowledgment. The authors gratefully acknowledge that this work was supported by Korea Research Foundation Grant funded by Korean Government (MOEHRD) (project no. R08-2003-000-10858-0).

References and Notes

(1) Choi, S. U. S. *ASME FED* **1995**, *231*, 99.
(2) Lee, S.; Choi, S. U. S.; Li, S.; Eastman, J. A. *J. Heat. Transfer* **1999**, *121*, 280−289.
(3) Das, S. K.; Putra, N.; Thiesen, P.; Roetzel, W. *J. Heat Transfer* **2003**, *125*, 567−574.
(4) Mursshed, S. M. S.; Leong, K. C.; Yang, C. *Int. J. Therm. Sci.* **2005**, *44*, 367−373.
(5) Eastman, J. A.; Choi, S. U. S.; Li, S.; Yu, W.; Thompson, L. J. *Appl. Phys. Lett.* **2001**, *78*, 718−720.
(6) Xuan, Y.; Li, Q. *Int. J. Heat Fluid Flow* **2000**, *21*, 58−64.
(7) Patel, H. E.; Das, S. K.; Sundararajan, T.; Nair, A. S.; George, B.; Pradeep, T. *Appl. Phys. Lett.* **2003**, *83*, 2931−2934.
(8) Xie, H.; Wang, J.; Xi, T.; Liu, Y. *Int. J. Thermophys.* **2002**, *23*, 571−580.
(9) Choi, S. U. S.; Zhang, Z. G.; Yu, W.; Lockwood, F. E.; Grulke, E. A. *Appl. Phys. Lett.* **2001**, *79*, 2252.
(10) Xie, H.; Lee, H.; Youn, W.; Choi, M. *J. Appl. Phys.* **2003**, *94*, 4967−4971.
(11) Xuan, Y.; Li, Q.; Hu, W. *AIChE J.* **2003**, *49*, 1038−1043.
(12) Wang, B.-X.; Zhou, L.-P.; Peng, X.-F. *Int. J. Heat Mass Transfer* **2003**, *46*, 2665−2672.
(13) Keblinski, P.; Phillpot, S. R.; Choi, S. U. S.; Eastman, J. A. *Int. J. Heat Mass Transfer* **2002**, *45*, 855−863.
(14) Jang, S. P.; Choi, S. U. S. *Appl. Phys. Lett.* **2004**, *84*, 4316−4318.
(15) Kumar, D. H.; Patel, H. E.; Kumar, V. R. R.; Sundararajan, T.; Pradeep, T.; Das, S. K. *Phys. Rev. Lett.* **2004**, *93*, 144301.
(16) Xue, Q.; Xu, W.-M. *Mater. Chem. Phys.* **2005**, *90*, 298−301.
(17) Yu, W.; Choi, S. U. S. *J. Nanopart. Res.* **2003**, *5*, 167−171.
(18) Hunter, R. J. *Foundations of Colloid Science*, 1st ed.; Clarendon Press: Oxford, 1987.
(19) Kallay, N.; Zalac, S. *Croat. Chem. Acta* **2001**, *74*, 479−497.
(20) Nagasaka, Y.; Nagashima, A. *J. Phys. E: Sci. Instrum.* **1981**, *14*, 1435−1440.
(21) Parks, G. A. *Chem. Rev.* **1965**, *65*, 177−198.
(22) Bergstrom, L. *Adv. Colloid Interface* **1997**, *70*, 125−169.
(23) Xue, L.; Keblinski, P.; Phillpot, S. R.; Choi, S. U. S.; Eastman, J. A. *J. Chem. Phys.* **2003**, *118*, 337−339.